Explicit and Implicit TVD and ENO High Resolution Algorithms Applied to the Euler and Navier-Stokes Equations in Three-Dimensions – Turbulent Results

EDISSON SÁVIO DE GÓES MACIEL
IEA – Aeronautical Engineering Division
ITA – Aeronautical Technological Institute
Praça Mal. Eduardo Gomes, 50 – Vila das Acácias – São José dos Campos – SP – 12228-900
BRAZIL
edissonsavio@yahoo.com.br http://www.edissonsavio.eng.br

Abstract: - In the present work, the Harten and Osher TVD/ENO and the Yee TVD symmetric schemes are implemented, on a finite volume context and using a structured spatial discretization, to solve the laminar/turbulent Navier-Stokes equations in the three-dimensional space. The Harten and Osher TVD/ENO schemes are flux difference splitting type, whereas the Yee TVD scheme is a symmetric one, which incorporates TVD properties due to the appropriated definition of a limited dissipation function. All three schemes are second order accurate in space. Turbulence is taken into account considering two algebraic models, namely: the Cebeci and Smith and the Baldwin and Lomax ones. A spatially variable time step procedure is also implemented aiming to accelerate the convergence of the algorithms to the steady state solution. The gains in convergence with this procedure were demonstrated in Maciel. The schemes are applied to the solution of the physical problem of the low supersonic flow along a ramp. The results have demonstrated that the most accurate results are obtained with the Harten and Osher ENO scheme. This paper is the third part of this work, TURBULENT RESULTS, considering the description of the turbulence models and the solutions obtained with them and compared with the laminar results.

Key-Words: - Harten and Osher algorithm, TVD/ENO formulations, Yee symmetric algorithm, TVD formulation, Euler and Navier-Stokes equations, Turbulence models, Explicit and implicit algorithms, Finite Volumes.

1 Introduction

In the present work, the [1] TVD/ENO and the [2] TVD symmetric schemes are implemented, on a finite volume context and using a structured spatial discretization, to solve the laminar/turbulent Navier-Stokes equations in the three-dimensional space. The [1] TVD/ENO schemes are flux difference splitting type, whereas the [2] TVD scheme is a symmetric one, which incorporates TVD properties due to the appropriated definition of a limited dissipation function. All schemes are second order accurate in space and their numerical implementation is based on the concept of [3]'s modified flux function. Turbulence is taken into account considering two algebraic models, namely: the [4-5] ones. The viscous simulations are treated with the explicit versions of the present algorithms, which employ a time splitting method ([6]). The schemes are accelerated to the steady state solution using a spatially variable time step procedure, which has demonstrated effective gains in terms of convergence rate ([7-8]). The algorithms are applied to the solution of the physical problem of the supersonic flow along a ramp. The results have demonstrated that the most accurate results are obtained with the [1] ENO scheme. The inviscid and laminar results are presented in [9].

The main contribution of the present work to the CFD (Computational Fluid Dynamics) community is the extension of the [1] TVD/ENO schemes, as well as the [2] TVD symmetric scheme, to three-dimensions, following a finite volume context, and their implementation coupled with two different turbulence algebraic models to simulate viscous turbulent flows, which characterizes an original contribution in the field of high resolution structured numerical algorithms. Details of the numerical implementation of the present algorithms are described in [6].

2 Turbulence Models

2.1 Turbulence model of [4]

The problem of the turbulent simulation is in the calculation of the Reynolds stress. Expressions involving velocity fluctuations, originating from the

averaging process, represent six new unknowns. However, the number of equations remains the same and the system is not closed. The modelling function is to develop approximations to these correlations. To the calculation of the turbulent viscosity according to the [4] model, the boundary layer is divided in internal and external.

Initially, the (ν_w) kinematic viscosity at wall and the ($\tau_{xy,w}$) wall shear stress are calculated. After that, the (δ) boundary layer thickness, the (δ_{LM}) linear momentum thickness and the (Vt_{BL}) boundary layer tangential velocity are calculated. So, the (N) normal distance from the wall to the studied cell is calculated. The N^+ term is obtained from:

$$N^+ = \sqrt{\mathrm{Re}}\sqrt{\tau_{xy,w}/\rho_w}\, N/\nu_w , \quad (1)$$

where ρ_w is the wall density and Re is the laminar Reynolds number. The van Driest damping factor is calculated by:

$$D = 1 - e^{(-N^+\sqrt{\rho/\rho_w}\,\mu_w/\mu/A^+)} , \quad (2)$$

with A^+ = 26, ρ is the fluid density and μ is the molecular viscosity. After that, the (dVt/dN) normal to the wall gradient of the tangential velocity is calculated and the internal turbulent viscosity is given by:

$$\mu_{Ti} = \mathrm{Re}\rho(\kappa N D)^2\, dVt/dN , \quad (3)$$

where κ is the von Kárman constant, which has the value 0.4. The intermittent function of Klebanoff is calculated to the external viscosity by:

$$g_{Kleb}(N) = \left[1 + 5.5(N/\delta)^6\right]^{-1} . \quad (4)$$

With it, the external turbulent viscosity is calculated by:

$$\mu_{Te} = \mathrm{Re}(0.0168)\rho Vt_{BL}\delta_{LM} g_{Kleb} . \quad (5)$$

Finally, the turbulent viscosity is chosen from the internal and the external viscosities: $\mu_T = MIN(\mu_{Ti}, \mu_{Te})$.

2.1 Turbulence model of [5]

To the calculation of the turbulent viscosity according to the [5] model, the boundary layer is again divided in internal and external. In the internal layer,

$$\mu_{Ti} = \rho l_{mix}^2 \|\omega\| \quad \text{and} \quad l_{mix} = \kappa N\left(1 - e^{-N^+/A_0^+}\right). \quad (6)$$

In the external layer,

$$\mu_{Te} = \rho\alpha C_{cp} F_{wake} F_{Kleb}(N; N_{\max}/C_{Kleb}) , \quad (7)$$

with:

$$F_{wake} = MIN\left[N_{\max} F_{\max}; C_{wk} N_{\max} U_{dif}^2 / F_{\max}\right] \quad \text{and}$$
$$F_{\max} = 1/\kappa\left[\underset{N}{MAX}\left(l_{mix}\|\omega\|\right)\right]. \quad (8)$$

Hence, $N_{\max}$ is the value of N where $l_{mix}\|\omega\|$ reached its maximum value and l_{mix} is the Prandtl mixture length. The constant values are: $\kappa = 0.4$, $\alpha = 0.0168$, $A_0^+ = 26$, $C_{cp} = 1.6$, $C_{Kleb} = 0.3$ and $C_{wk} = 1$. F_{Kleb} is the intermittent function of Klebanoff given by:

$$F_{Kleb}(N) = \left[1 + 5.5(C_{Kleb} N/N_{\max})^6\right]^{-1} , \quad (9)$$

$\|\omega\|$ is the magnitude of the vorticity vector and U_{dif} is the difference between the maximum velocity value at N and the value of velocity at $N = N_{max}$ in the boundary layer case:

$$U_{dif} = \left(\sqrt{u^2 + v^2 + w^2}\right)_{\max} - \left(\sqrt{u^2 + v^2 + w^2}\right)_{N = N_{\max}} . \quad (10)$$

3 Results

Tests were performed in a microcomputer with processor AMD SEMPRON (tm) 2600+, 1.83GHz, and 512 Mbytes of RAM. As the interest of this work is steady state problems, one needs to define a criterion which guarantees that such condition was reached. The criterion adopted in this work was to consider a reduction of 3 orders in the magnitude of the maximum residual in the domain, a typical criterion in the CFD community. The residual was defined in [9], as well the procedure to determine the maximum one in the numerical field. The upstream flow angle was set equal to 0.0°. At the same time, the angle at the longitudinal plane was also set equal to 0.0°. All pressure distributions were determined at the plane corresponding to k = KMAX/2, where "KMAX" is the maximum number of points in the z direction, and j = 1, corresponding to the configuration wall.

To the turbulent case studied in this work, the explicit version of the numerical algorithms was

used. It is important to remember from [9] the nomenclature employed to the Yee's variants: Min1 (minmod1), Min2 (minmod2), Min3 (minmod3), SB (Super Bee), and VL (Van Leer). The initial and boundary conditions are described in [10].

3.1 Viscous turbulent results

In the viscous studies only simulations with the [1] ENO and TVD versions and [2] Min1 and Min2 versions yielded converged results. The other limiters due to the [2] scheme did not produce steady state solutions.

The physical problem studied in the viscous turbulent simulations is the flow along a ramp. The xy plane configuration and the employed mesh are described in [9]. This problem is a supersonic flow hitting a ramp with 20° of inclination. It generates a shock and an expansion fan. The freestream Mach number adopted as initial condition to this simulation was 2.0, characterizing a low supersonic flow. The Reynolds number was estimated to be 1.613×10^5, as evaluated in [9].

3.1.1 [4] Results

Figures 1 to 4 show the pressure contours obtained by the [1] ENO, [1] TVD, [2] TVD Min1 and [2] TVD Min2 schemes, respectively. The most severe pressure field was obtained by the [1] TVD scheme using the [4] model. As can be observed, the weaker shock wave formed before the ramp in the laminar solutions ([9]) practically did not appear in the solution generated by the [1] TVD scheme, indicating that the separated region should be very small in this solution if not vanished. In all solutions, the extension of the separation region detected in the turbulent solution is reduced. It ratifies the behaviour observed in the boundary layer literature that in turbulent flows, the extension of the separated region is smaller than the respective one in laminar flows. It is because of the turbulent effects that energize the boundary layer, does not allowing that any instability of the flow causes the breakdown of the boundary layer stability.

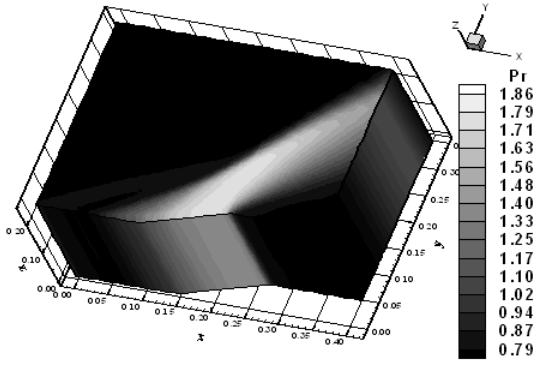

Figure 1 : Pressure contours ([1]-ENO).

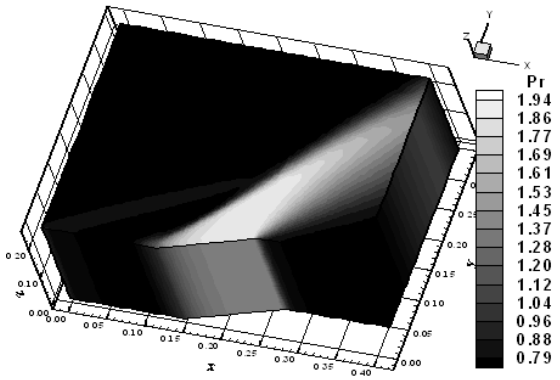

Figure 2 : Pressure contours ([1]-TVD).

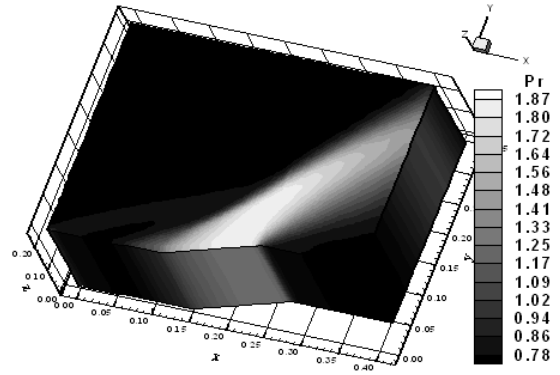

Figure 3 : Pressure contours ([2]-Min1).

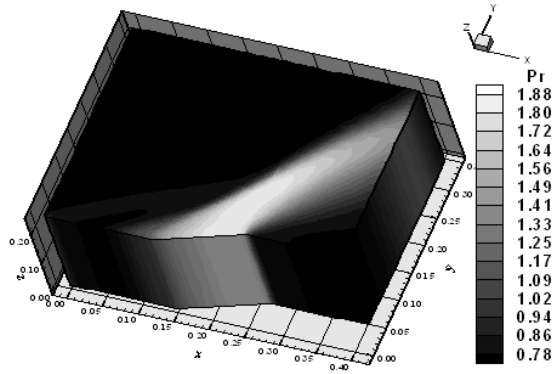

Figure 4 : Pressure contours ([2]-Min2).

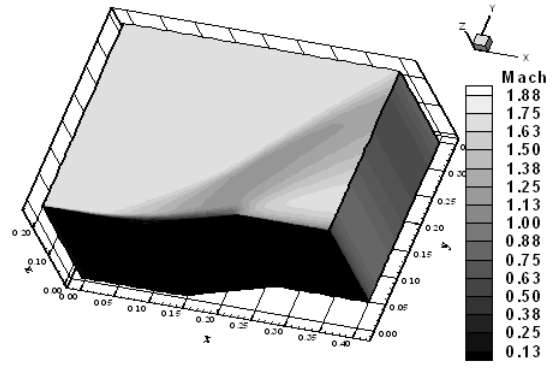

Figure 5 : Mach number contours ([1]-ENO).

Figures 5 to 8 exhibit the Mach number contours obtained by the schemes of [1] ENO, of [1] TVD, of

[2] TVD Min1 and of [2] TVD Min2, respectively. The most intense Mach number fields are obtained by the [2] TVD Min1 and Min2 variants using the [4] model in relation to the ones due to [1]. Again the weaker shock wave is practically not perceived in the [1] TVD solution.

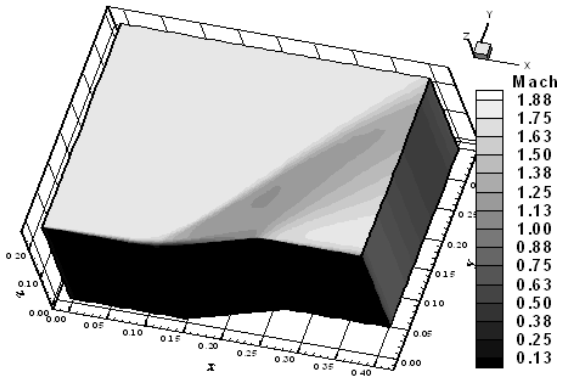

Figure 6 : Mach number contours ([1]-TVD).

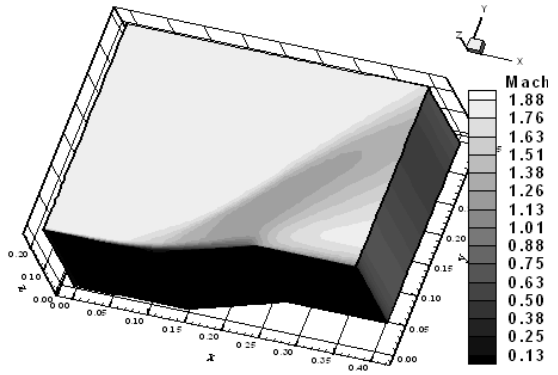

Figure 7 : Mach number contours ([2]-Min1).

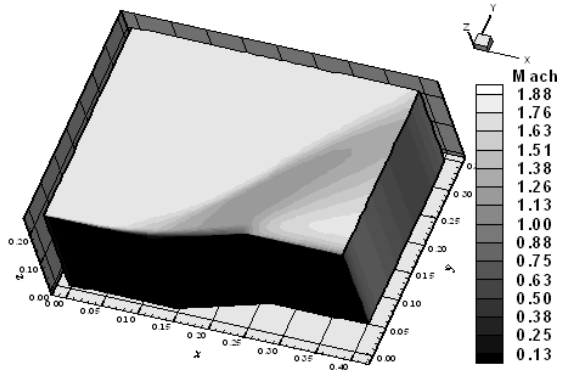

Figure 8 : Mach number contours ([2]-Min2).

Figures 9 to 12 present the velocity vector fields and the streamlines obtained by each scheme close to the ramp wall. It is possible to observe that all schemes detect the separation region with the formation of a circulation bubble. However, the [1] TVD scheme detects the minimum extension of separated flow, indicating that this scheme respect the main features of the turbulence model of [4], predicting less severe regions of separation and of loss of energy and pressure.

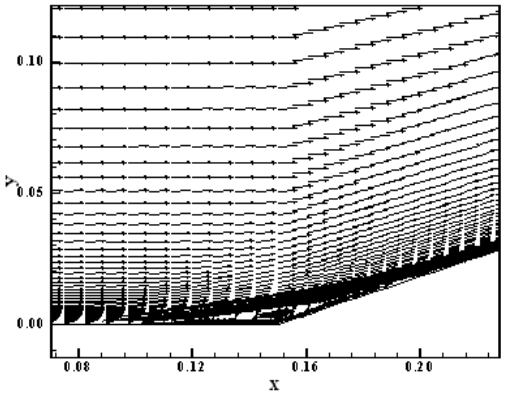

Figure 9 : Velocity field and streamlines ([1]-ENO).

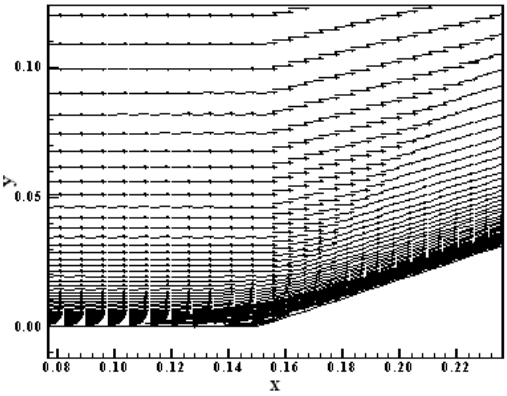

Figure 10 : Velocity field and streamlines ([1]-TVD).

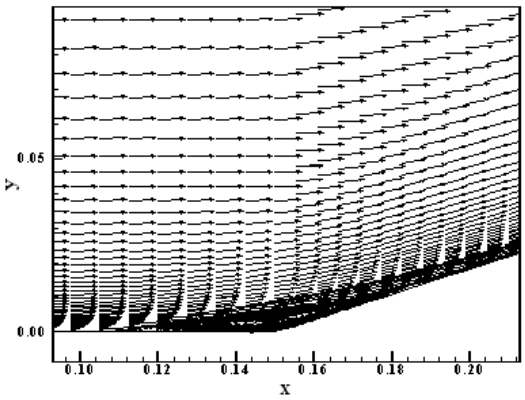

Figure 11 : Velocity field and streamlines ([2]-Min1).

As observed in [9], one way to quantitatively verify if the solutions generated by each scheme are satisfactory consists in determining the shock angle of the oblique shock wave, β, measured in relation to the initial direction of the flow field. The viscosity affects the shock angle due to the smearing of the shock wave close to the ramp corner. The shock wave is diffused at this region causing a variation in the determination of the shock angle.

[11] (pages 352 and 353) presents a diagram with values of the shock angle, β, to oblique shock waves. The value of this angle is determined as function of the freestream Mach number and of the deflection angle of the flow after the shock wave, ϕ. To the ramp problem, ϕ = 20º (ramp inclination angle) and the freestream Mach number is 2.0, resulting from this diagram a value to β equals to 53.0º.

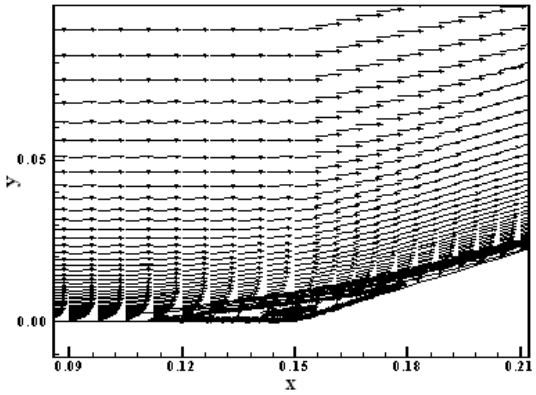

Figure 12 : Velocity field and streamlines ([2]-Min2).

Using a transfer in Figures 1 to 4, considering the xy plane, it is possible to obtain the values of β to each scheme, as well the respective errors, shown in Tab. 1. As can be observed, the best scheme was the [1] ENO scheme.

Table 1 : Shock angle and respective percentage errors ([4]).

Algorithm	β(°)	Error (%)
[1] ENO	52.20	1.51
[1] TVD	54.50	2.83
[2] TVD Min1	53.90	1.70
[2] TVD Min2	54.00	1.89

3.1.2 [5] Results

Figures 13 to 16 exhibit the pressure contours obtained by the [1] ENO, the [1] TVD, the [2] TVD Min1 and the [2] TVD Min2, respectively. The most severe pressure field is obtained with the [2] TVD Min2 using the [5] model. Again, the weaker shock wave is perceptible in all solutions, indicating that the [5] model is not able to suppress the boundary layer detachment or to reduce the boundary layer separation as the [4] does.

Figures 17 to 20 show the Mach number contours obtained by the schemes of [1] ENO, of [1] TVD, of [2] TVD Min1 and of [2] TVD Min2, respectively. The most intense Mach number field is obtained by the [2] TVD Min1 scheme. The weaker shock wave due to the raise in the boundary layer thickness is again perceptible.

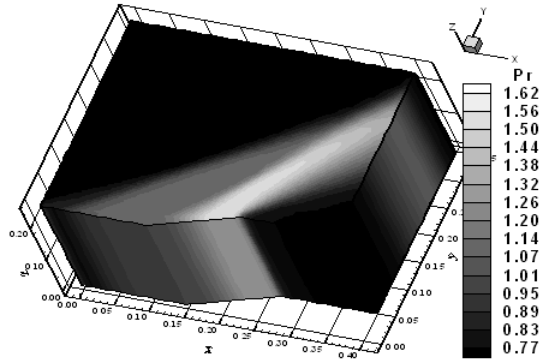

Figure 13 : Pressure contours ([1]-ENO).

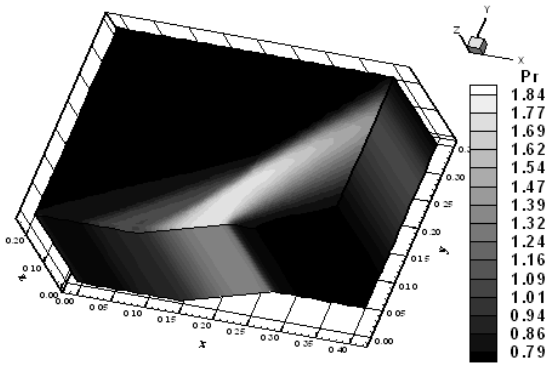

Figure 14 : Pressure contours ([1]-TVD).

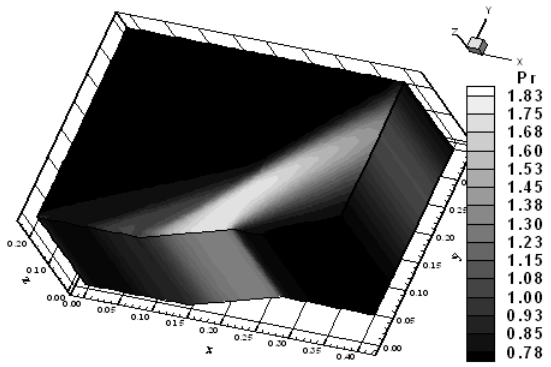

Figure 15 : Pressure contours ([2]-Min1).

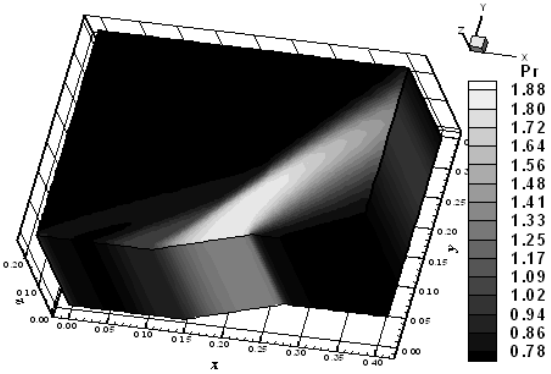

Figure 16 : Pressure contours ([2]-Min2).

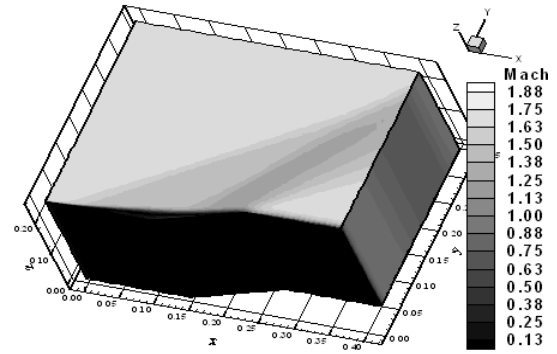

Figure 17 : Mach number contours ([1]-ENO).

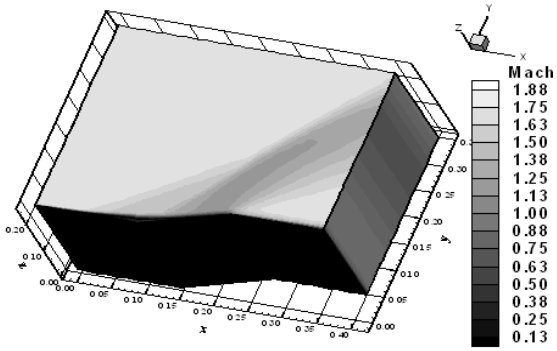

Figure 18 : Mach number contours ([1]-TVD).

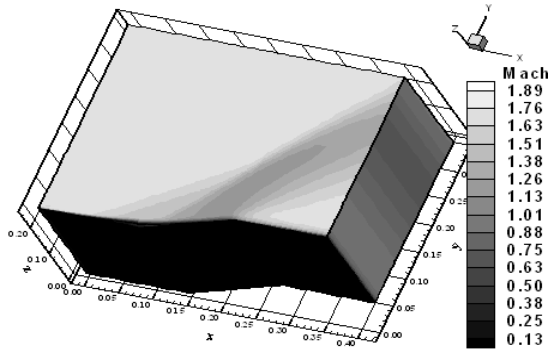

Figure 19 : Mach number contours ([2]-Min1).

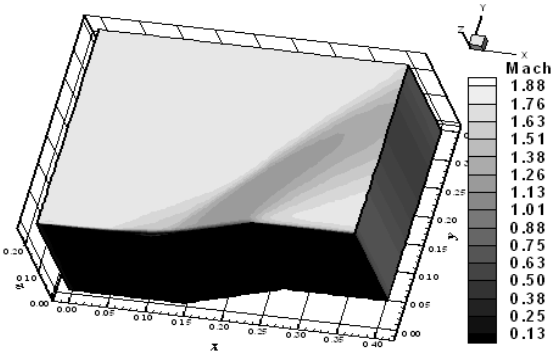

Figure 20 : Mach number contours ([2]-Min2).

Figures 21 to 24 present the velocity vector fields and the streamlines obtained by each scheme close to the ramp wall. It is possible to observe that all schemes detect the separation region with the formation of a circulation bubble. However, all schemes detect regions of separated flow bigger than the respective ones obtained with the [4] model. Apparently, the [5] model agrees with the laminar behaviour, while the [4] model predicts less severe regions of turbulence with all algorithms.

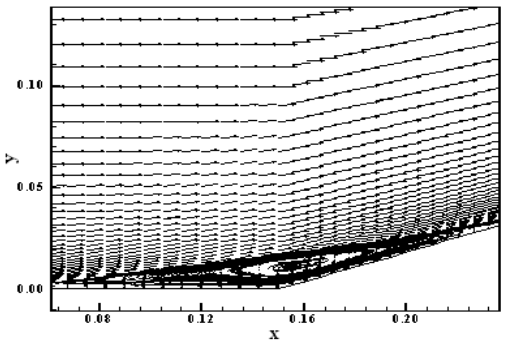

Figure 21 : Velocity field and streamlines ([1]-ENO).

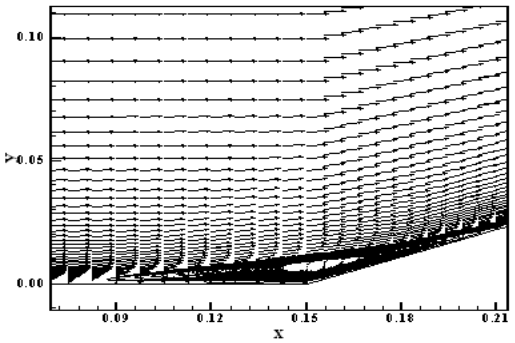

Figure 22 : Velocity field and streamlines ([1]-TVD).

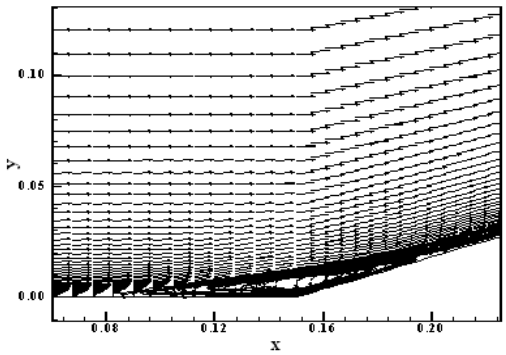

Figure 23 : Velocity field and streamlines ([2]-Min1).

Again, it is possible to determine by each scheme the shock angle of the oblique shock wave, β, measured in relation to the initial direction of the flow field. Using a transfer in Figures 13 to 16, considering the xy plane, it is possible to obtain the values of β to each scheme, as well the respective errors, shown in Tab. 2. As can be observed, the [1] ENO and TVD schemes are better than the [2] TVD symmetric variants, because of the limiters that are

used in the former scheme, better designed to compressible flows.

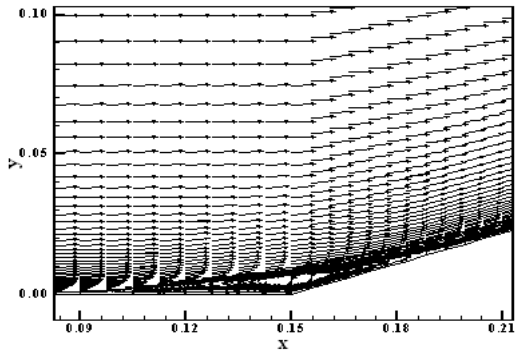

Figure 24 : Velocity field and streamlines ([2]-Min2).

Table 2 : Shock angle and respective percentage errors ([5]).

Algorithm	β(°)	Error (%)
[1] ENO	52.00	1.89
[1] TVD	54.00	1.89
[2] TVD Min1	51.40	3.02
[2] TVD Min2	55.00	3.77

3.2 Comparisons among wall pressure distributions, detachment and reattachment points of the boundary layer, oblique shock angles and simulation data

Figure 25 shows the laminar wall pressure distributions ([9]) obtained by the [1] ENO, the [1] TVD, the [2] TVD Min1 and the [2] TVD Min2 schemes. These wall pressure distributions are compared with the inviscid solution, which is the true solution according to the boundary layer theory.

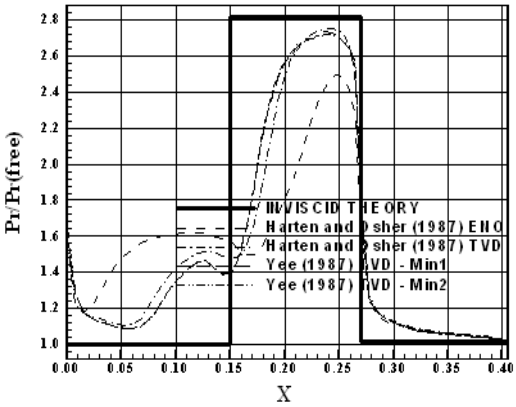

Figure 25 : Wall pressure distributions (Laminar).

As can be observed, the [1] ENO scheme presents the largest region of flow separation and is the most smeared in relation to the other schemes. The closest distribution in relation to the inviscid case is obtained from the [1] TVD scheme. In Figure 26, the wall pressure distributions obtained by the schemes using the [4] model present small regions of separation and values of maximum pressure closer to the inviscid solution, being the solution generated by the [1] TVD scheme again the closest to the solution predicted by the boundary layer theory.

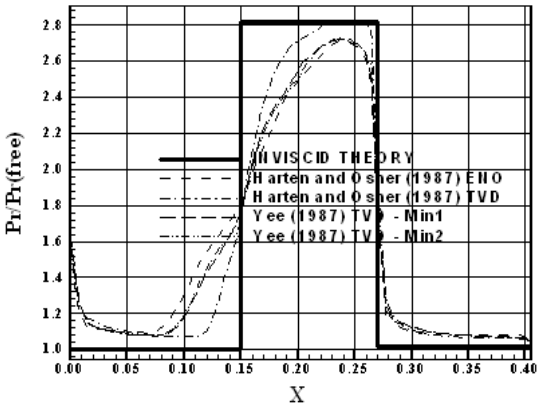

Figure 26. Wall pressure distributions ([4]).

Figure 27 shows the wall pressure distributions generated by the all four schemes using the [5] model. Again, a bigger region of separated flow is perceptible in all solutions, with bigger extension in the solution generated by the [1] ENO scheme. The better pressure distribution, in accordance with the boundary layer theory, is due to [2] TVD Min2 scheme.

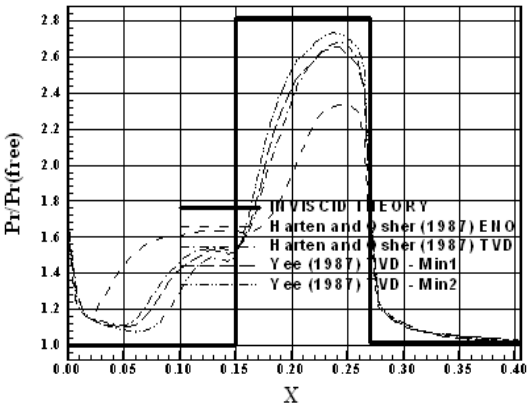

Figure 27. Wall pressure distributions ([5]).

Figure 28 shows all wall pressure distributions obtained by the [1] ENO scheme, in all cases, laminar and turbulent. As can be observed, the best distribution occurred as the [4] model was employed. Figure 29 exhibits the wall pressure distributions generated by the [1] TVD scheme to the three cases, laminar and the two turbulence models, compared with the theory of boundary layer

and the best solution was again obtained by the [4] model. Figure 30 presents the wall pressure distribution obtained by the [2] TVD Min1 scheme to the three studied cases. The [4] model and the laminar solutions were closer to the theoretical result. Finally, Figure 31 presents better pressure distributions generated by the [2] TVD Min2 scheme in the laminar case and using the [4] model.

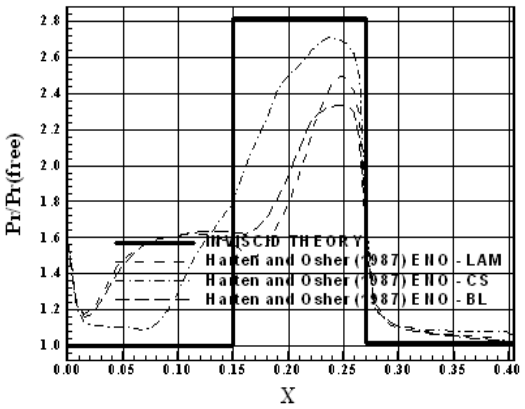

Figure 28 : Wall pressure distributions ([1]-ENO).

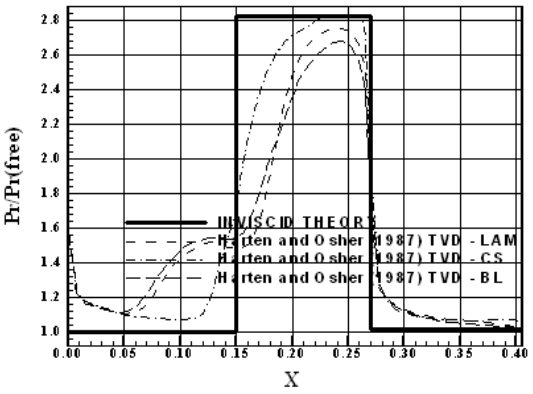

Figure 29 : Wall pressure distributions ([1]-TVD).

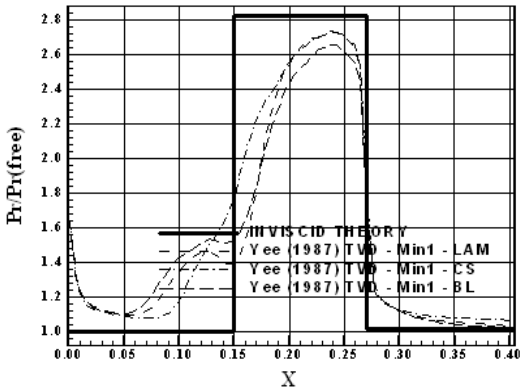

Figure 30 : Wall pressure distributions ([2]-Min1).

Table 3 presents the points of detachment and reattachment involving the laminar and turbulent cases to the four algorithms tested in these viscous simulations.

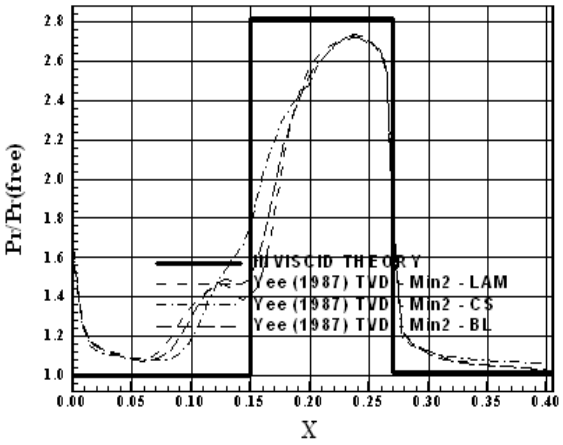

Figure 31 : Wall pressure distributions ([2]-Min2).

Analysing this table, it is possible to highlight that the [2] TVD Min2 scheme presents the minimum region of separated flow in comparison with the other schemes in all three possible cases studied in this work. As the behaviour expected for the turbulence model is to reduce the extension of the separation region due to better equilibrium characteristics inherent to turbulent boundary layers, the [2] TVD Min2 scheme reaches such goal satisfactorily in theoretical terms.

Table 3 : Boundary layer detachment and reattachment points.

Laminar	[1] ENO	[1] TVD	[2] Min1	[2] Min2
Det.(1) (m)	0.05	0.08	0.09	0.10
Reat.(2)(m)	0.25	0.20	0.20	0.20
[4]	[1] ENO	[1] TVD	[2] Min1	[2] Min2
Det. (m)	0.10	0.12	0.12	0.12
Reat. (m)	0.20	0.18	0.18	0.18
[5]	[1] ENO	[1] TVD	[2] Min1	[2] Min2
Det. (m)	0.08	0.09	0.09	0.10
Reat. (m)	0.22	0.20	0.20	0.20

(1): Detachment; (2): Reattachment.

Table 4 : Shock angle obtained in the laminar and turbulent cases.

Laminar	[1] ENO	[1] TVD	[2] Min1	[2] Min2
β (°)	48.00	54.20	53.00	52.80
Error (%)	9.43	2.26	0.00	0.38
[4]	[1] ENO	[1] TVD	[2] Min1	[2] Min2
β (°)	52.20	54.50	53.90	54.00
Error (%)	1.51	2.83	1.70	1.89
[5]	[1] ENO	[1] TVD	[2] Min1	[2] Min2
β (°)	52.00	54.00	51.40	55.00
Error (%)	1.89	1.89	3.02	3.77

Aiming a global comparison involving the shock angle of the oblique shock waves estimated by the

schemes in these viscous simulations, Tab. 4 exhibits the values of these angles and respective errors. As can be observed, the [1] ENO scheme presents more accurate values of the angle of the oblique shock wave in two of the three studied cases (in both turbulent cases). The global error was less than 4.0% to all schemes, except to the [1] ENO scheme in the laminar case.

Table 5 shows the computational data of the numerical simulations in the viscous laminar and turbulent cases in the ramp problem. All four schemes to the viscous laminar and turbulent cases used an explicit formulation to the simulations. As observed, the fastest scheme is due to [1] TVD algorithm in all cases.

Table 5 : Computational data of the explicit algorithms to the ramp viscous cases.

	Laminar		[4]		[5]	
Scheme	CFL	Iter.(1)	CFL	Iter.	CFL	Iter.
[1] ENO	0.9	3,515	0.9	3,141	0.9	4,160
[1] TVD	0.9	1,755	0.9	955	0.9	2,094
[2] TVD – Min1	0.5	3,374	0.5	4,632	0.5	4,342
[2] TVD – Min2	0.5	3,026	0.5	4,657	0.5	3,438

(1): Iterations.

Table 6 exhibits the computational costs of the numerical algorithms obtained in the viscous laminar and turbulent cases. The cheapest algorithm in the laminar case is due to [2] TVD Min2, while the most expensive is due to [1] ENO. In the turbulent case, using the [4] model, the cheapest algorithm is due to [2] TVD Min1, while the most expensive is again due to [1] ENO. Finally, using the [5] model, the cheapest algorithm is the [2] TVD Min2 scheme, while the most expensive is again the [1] ENO scheme. As conclusion, in general the [2] TVD Min2 scheme yields the cheapest one in terms of viscous laminar and turbulent simulations.

Table 6. Computational cost of the numerical algorithms (laminar and turbulent cases).

	Computational Cost(1)		
Scheme	Laminar	[4]	[5]
[1] ENO	0.0000779	0.0001612	0.0000915
[1] TVD	0.0000744	0.0001548	0.0000885
[2] TVD Min1	0.0000694	0.0001523	0.0000843
[2] TVD Min2	0.0000692	0.0001524	0.0000841

(1): Measured in seconds/per cell/per iterations.

4 Conclusions

In the present work, the [1] TVD/ENO and the [2] TVD symmetric schemes are implemented, on a finite volume context and using a structured spatial discretization, to solve the laminar/turbulent Navier-Stokes equations in the three-dimensional space. The [1] TVD/ENO schemes are flux difference splitting type, whereas the [2] TVD scheme is a symmetric one, which incorporates TVD properties due to the appropriated definition of a limited dissipation function. All schemes are second order accurate in space and their numerical implementation is based on the concept of [3]'s modified flux function. Turbulence is taking into account considering two algebraic models, namely: the [4-5] ones. The viscous simulations are treated with the explicit versions of the present algorithms, which employ a time splitting method ([6]). The schemes are accelerated to the steady state solution using a spatially variable time step procedure, which has demonstrated effective gains in terms of convergence rate ([7-8]). The algorithms are applied to the solution of the physical problem of the low supersonic flow along a ramp.

The results have demonstrated that the most accurate results are obtained with the [1] ENO scheme. In the inviscid case ([9]), it is possible to highlight that the [2] TVD VL scheme yields the best pressure distribution along the nozzle lower wall. In the compression corner, the [1] ENO and TVD schemes present better pressure distributions than those generated by the [2] TVD schemes. The [2] TVD Min1, Min2, Min3 and VL variants present oscillations in the pressure distributions. The shock angle of the oblique shock wave that is formed at the compression corner is best estimated by the [1] ENO and [2] TVD VL algorithms. The most expensive tested implicit scheme was due to [1] ENO scheme, while the cheapest was the [2] TVD Min2 scheme. The former is approximately 172.91% more expensive than the latter.

In the ramp viscous case, the laminar results ([9]) present the [2] TVD Min1 scheme as yielding the best value to the shock angle at the ramp. In the turbulent case, present paper, the [4] model presents the [1] ENO scheme as yielding the best estimation, while in the [5] model, the [1] ENO and TVD schemes produce the best values to the shock angle. In the laminar case, the [1] ENO scheme presents the biggest separation region with the formation of a circulation bubble. The best pressure distribution, closest with the inviscid solution - true solution considering the boundary layer theory -, was obtained by the [1] TVD scheme. Employing the [4] model, all tested algorithms present the minimum

separation region, with this model energizing the boundary layer sufficiently to guarantee the minimum circulation region. Again, the [1] TVD scheme presents the pressure distribution at the wall closest with inviscid solution. With the [5] model, the best pressure distribution is obtained by the [2] TVD Min2 algorithm - in relation to the inviscid solution). The minimum region of separation was obtained by the [2] TVD Min2 scheme in all three cases (laminar and the two turbulent cases). Considering the values estimated by the shock angle of the oblique shock wave, the [1] ENO algorithm presents the best values to this parameter in two of the three cases – in the two turbulent cases. As general conclusion in terms of viscous simulations, all algorithms present the best solution considering wall pressure distribution as using the [4] model.

5 Acknowledgments

The present author acknowledges the CNPq by the financial support conceded under the form of a DTI (Industrial Technological Development) scholarship no. 384681/2011-5. He also acknowledges the infra-structure of the ITA that allowed the realization of this work.

References:

[1] A. Harten, and S. Osher, Uniformly High-Order Accurate Nonoscillatory Schemes I, *SIAM Journal on Numerical Analysis*, Vol. 24, No. 2, 1987, pp. 279-309.

[2] H. C. Yee, Construction of Explicit and Implicit Symmetric TVD Schemes and Their Applications, *Journal of Computational Physics*, Vol. 68, 1987, pp. 151-179.

[3] A. Harten, High Resolution Schemes for Hyperbolic Conservation Laws, *Journal of Computational Physics*, Vol. 49, No. 2, 1983, pp. 357-393.

[4] T. Cebeci, and A. M. O. Smith, A Finite-Difference Method for Calculating Compressible Laminar and Turbulent Boundary Layers, *Journal of Basic Engineering, Trans. ASME*, Series B, Vol. 92, No. 3, 1970, pp. 523-535.

[5] B. D. Baldwin, and H. Lomax, Thin Layer Approximation and Algebraic Model for Separated Turbulent Flows, *AIAA Paper 78-257*, 1978.

[6] E. S. G. Maciel, Explicit and Implicit TVD and ENO High Resolution Algorithms Applied to the Euler and Navier-Stokes Equations in Three-Dimensions – Theory", *Proceedings of the XX International Congress of Mechanical Engineering (XX COBEM)*, Gramado, RS, Brazil, 2009.

[7] E. S. G. Maciel, Analysis of Convergence Acceleration Techniques Used in Unstructured Algorithms in the Solution of Aeronautical Problems – Part I, *Proceedings of the XVIII International Congress of Mechanical Engineering (XVIII COBEM)*, Ouro Preto, MG, Brazil, 2005.

[8] E. S. G. Maciel, Analysis of Convergence Acceleration Techniques Used in Unstructured Algorithms in the Solution of Aerospace Problems – Part II, Proceedings of the XII Brazilian Congress of Thermal Engineering and Sciences (XII ENCIT), Belo Horizonte, MG, Brazil, 2008.

[9] E. S. G. Maciel, Explicit and Implicit TVD and ENO High Resolution Algorithms Applied to the Euler and Navier-Stokes Equations in Three-Dimensions – Results, *Proceedings of the XX International Congress of Mechanical Engineering (XX COBEM)*, Gramado, RS, Brazil, 2009.

[10] E. S. G. Maciel, Relatório ao Conselho Nacional de Pesquisa e Desenvolvimento Tecnológico (CNPq) sobre as Atividades de Pesquisa Desenvolvidas no Terceiro Ano de Vigência da Bolsa de Estudos para Nível DCR-IF Referente ao Processo No. 304318/2003-5, *Report to the National Council of Scientific and Technological Development (CNPq)*, Recife, PE, Brazil, 52p, 2006. [Available at the website www.edissonsavio.eng.br]

[11] J. D. Anderson Jr., *Fundamentals of Aerodynamics*, McGraw-Hill, Inc., EUA, 563p, 1984.